Identification of Barium-Site Substitution of $BiFeO_3$-$Bi_{0.5}K_{0.5}TiO_3$ Multiferroic Ceramics: X-ray Absorption Near Edge Spectroscopy

Anurak Prasatkhetragarn[a,b,*], Jaru Jutimoosik[c], Pongsakorn Jantaratana[d],

Pinit Kidkhunthod[e], Rattikorn Yimnirun[f] and James Ren[g]

[a]*Department of Materials Science, School of Science, University of Phayao, Phayao 56000, Thailand*
[b]*Unit of Excellence on Sensors Technology, University of Phayao, Phayao 56000, Thailand*
[c]*Department of Physics, Faculty of Science, Naresuan University, Phitsanulok 65000, Thailand*
[d]*Department of Physics, Faculty of Science, Kasetsart University, Bangkok 10900, Thailand*
[e]*Synchrotron Light Research Institute, Nakhon Ratchasima 30000, Thailand*
[f]*School of Energy Science and Engineering, Vidyasirimedhi Institute of Science and Technology (VISTEC), Rayong 21210, Thailand*
[g]*Department of Maritime and Mechanical Engineering, Liverpool John Moores University, Liverpool L3 3AF, UK*

** Email address of corresponding author: Prasatkhetragarn@yahoo.com (A. Prasatkhetragarn)*

Abstract

In this work, the effects of barium substitution on the local structure, dielectric and magnetic properties of the polycrystalline ceramics $0.6BiFeO_3$–$0.4(Bi_{0.5}K_{0.5})TiO_3$ (0.6BFO–0.4BKT) system was investigated. A solid-state reaction technique was used to synthesize the materials with barium (Ba) doping of 1, 3, 5, 7, and 10 mol%. XRD analysis reveals the coexistence between tetragonal and rhombohedral phases of single-phase perovskite in pure 0.6BFO–0.4BKT and the rhombohedral reach phase was found with increasing Ba content. XANES simulations indicate that the majority of Ba atoms occupy A-site in BKT lattice of Ba-doped 0.6BFO-0.4BKT, the oxidation state of Fe, Ti, and Ba ions are +3, +4 and +2, respectively. At 5 mol% of Ba doping content, the dielectric measurement shows the morphotropic phase boundary (MPB) and the maximum value of ferromagnetic characteristic were observed, indicating an optimum composition, properties and production conditions.

Keyword: X-Ray absorption near edge spectroscopy; Barium-doped; Multiferroic ceramics; XANES simulations

1. Introduction

Bismuth ferrite ($BiFeO_3$) is considered one of the most promising multiferroic materials for realizing the full potential of multiferroic devices. The material has a highly disordered ABO_3 perovskite-type rhombohedral structure following the space group *R*3*c* (lattice parameters of a = 0.5637 nm and c = 1.3802 nm) (Yoneda et al., 2012). The mechanism of ferroelectricity is essentially originated from the long-range ordering of dipolar moments on the Bi site. The spontaneous polarization (P_s) of $BiFeO_3$ was reported to be 84 μC/cm^2 based on theoretical calculation with a ferroelectric Curie temperature (T_C) of ~1,100 K and an antiferromagnetic Néel temperature (T_N) of

~640 K. Both ferroelectricity and antiferromagnetism have long been known in $BiFeO_3$ single crystals (Lee et al., 2008; Lebeugle et al., 2007). Recent studies of $BiFeO_3$ thin films have confirmed the existence of a large ferroelectric polarization and a small level magnetization, this was consistent with theoretical predictions (Zhao et al., 2006). Despite the identification of these promising functional properties, the bulk $BiFeO_3$ ceramic is difficult to prepare. Pure single-phase and pure $BiFeO_3$-based materials have a low electrical resistivity, which is the main factor preventing wide practical applications of $BiFeO_3$-based materials as piezoelectric or magnetoelectric functional components (Matsuo et al., 2010)

Several works have explored the development of new materials systems with improved functions and manufacturability. Some researchers have studied the $BiFeO_3$–$(Bi_{0.5}K_{0.5})TiO_3$ (BFO-BKT) solid solutions and investigated their ferroelectric and piezoelectric properties (Matsuo et al., 2010; Kim et al., 2010). In the work by Matsuo et al, BFO-BKT ceramics with various compositions were prepared by the flash creation method (FCM), the materials showed a large P_r (52 μC/cm^2), a superior piezoelectric d_{33} coefficient (130 pC/N), and a high phase transition temperature around 720 K at a composition of 0.6BFO–0.4BKT (Matsuo et al., 2010; Kim et al., 2010). The FCM is an effective technique to prepare metal-oxide nanopowders, in which vaporized raw materials are introduced into a plasma-induced high-temperature region and then cooled rapidly to crystallize without significant grain growth. The method could produce a lower concentration of defects in the ceramic powder with a lower sintering temperature compared to the conventional solid-state method (Wu et al., 2008). According to other reports, the 0.6BFO–0.4BKT ceramics prepared by the conventional solid-state reaction show no obvious ferroelectric switching and its P_r and d_{33} were very small (~10 μC/cm^2 and ~40 pC/N, respectively) even under high electric field amplitudes (Matsuo et al., 2010; Kim et al., 2010). This suggests that the ferroelectric and piezoelectric properties of the 0.6BFO–0.4BKT ceramics are highly dependent on the processing method. The control of the defect concentration is of great importance to obtain the superior properties of these ceramics. One effective way to control defect concentration by applying chemical modification using a small amount of oxide additive, which has been successfully applied to enhance the properties and functions of ceramics (Prasatkhetragarn et al., 2013; Dehkordi et al., 2014; Yang et al., 2017). Many current works are focused on using doping elements (Prasatkhetragarn et al., 2013; Han et al., 2013; Pan et al., 2016; Qin et al., 2018) in different material systems. For example, Pan et al., 2016 reported work on La-doped $BiFeO_3$ multiferroic thin films by magnetic-field-assisted scanning probe microscopy. Srinivas (Srinivas et al., 2016) studied the structural and magnetic properties of Mn-doped $BiFeO_3$ nanomaterials. Wang et al. (2017) investigated the temperature-dependent, large electromechanical strain in Nd-doped $BiFeO_3$-$BaTiO_3$ lead-free ceramics; Nguyen Hoang Tuan et al. (2017) reported the fabrication and properties of Co-doped $Bi_{0.5}K_{0.5}TiO_3$– $BiFeO_3$ solid solution. The use of barium

as the doping elements have been studied in some material systems such as $LaInO_3$ perovskite (Yoon et al., 2014), $BiFeO_3$ films (Vagadia et al., 2013) and Ba-doped InN (Xie et al., 2013). However, there have been no detailed studied on the local-structural around different elements, especially Ba atom on the Ba-doped BFO-BKT polycrystalline multiferroic ceramics within specific morphotropic phase boundary. Consequently, local structure, dielectric and magnetic properties of Ba-doped BFO-BKT Ceramics are investigated with X-ray Absorption Near Edge Spectroscopy, the influence of B-doping and optimum composition is established with an integrated experimental and computational study.

2. Experimental

Ba-doped $0.6BiFeO_3$–$0.4Bi_{0.5}K_{0.5}TiO_3$ (0.6BFO-0.4BKT) with 1, 3, 5, 7, and 10 mol% of Ba were prepared by a solid-state mechanical milling technique. Stoichiometric mixtures of starting reagent-grade oxides of $BaCO_3$ (Aldrich, 98.5%), Bi_2O_3 (Aldrich, 99.9%), K_2CO_3, (Aldrich, 99.9%), Fe_2O_3 (Aldrich, 99.9%) and TiO_2 (anatase structure) (Aldrich, 99.9%) were ball milled in ethanol with yttria-stabilized zirconia balls for 24 h. To achieve phase homogeneity, the powders were calcined in an alumina crucible at a temperature of 900 °C for 6 h (Kim et al., 2010; Prasatkhetragarn et al., 2013). The calcined powders with 3 wt.% PVA (polyvinyl alcohol) addition as a binder were then uniaxially pressed at 2500 psi into disc-shaped pellets with a diameter of 10 mm and a thickness of 1 mm. First step sintering was used to burnout PVA binder at 500 °C for 1 h, and then the pellets were sintered at 1025 °C for 2 h with a heating/cooling rate of 5 °C/min (Kim et al., 2010; Prasatkhetragarn et al., 2013). The phase structure of the ceramics was analyzed via X-ray diffraction (XRD; Philips XPert Pro). An Agilent 4284A LCR meter was used to measure the dielectric properties over a wide range of temperatures using a NorECS ProboStat high-temperature measurement cell. The room temperature ferromagnetic properties were determined using a Vibrating Sample Magnetometer (VSM). The experimental Fe, Ti K-edge and Ba L3-edge XANES spectra of Ba-doped BKT-BF samples were measured at beamline 5.2 (SUT-NANOTECH-SLRI, Siam Photon Laboratory, Synchrotron Light Research Institute (SLRI), Thailand). The Siam Photon storage ring was operated at an electron energy of 1.2 GeV and the electron beam current between 80-120 mA. A Ge (220) double crystal monochromator was used to select the X-ray photon energy. All XANES spectra were collected at the ambient temperature and atmospheric pressure. The spectra were measured in a fluorescent mode with a four-element Si drift detector. The normalized XANES data were processed and analyzed after background subtraction in the pre-edge and post-edge region using the ATHENA program (Ravel and Newville, 2005). The XANES spectra were also calculated by the FEFF8.2 program and qualitatively compared with the XANES patterns obtained from the experiment.

3. Results and discussion

XRD pattern of $0.6BiFeO_3$–$0.4Bi_{0.5}K_{0.5}TiO_3$ ceramics with 1, 3, 5, 7, and 10 mol% of Ba is shown in Fig. 1(a). The data shows that rhombohedral ($BiFeO_3$; JCPDS file no. 74- 2016) and tetragonal ($Bi_{0.5}K_{0.5}TiO_3$; JCPDS file no. 36-0339) phases coexist in the undoped of 0.6BFO–0.4BKT perovskite structure, which slightly shown a minor phase of $Bi_4Ti_3O_{12}$. However, the minor phase was removed by Ba dopant. The strongest reflections in (110) plane are slightly shifted indicating a distortion of the unit cell as shown in Fig. 1(b), this is possibly associated with Ba substation on the A-site of a normal ABO_3 perovskite structure.

To further quantify the effects of Ba on the structure of 0.6BFO-0.4BKT, the x-ray absorption near edge spectroscopy (XANES) of Fe *K*-edge, Ti *K*-edge, and Ba L_3-edge spectra are measured and discussed in order to establish the valence of Fe, Ti, and Ba, respectively. The normalized Fe and Ti *K*-edge XANES spectra and their first derivative of samples with different Ba content are compared with the standard of Fe_2O_3 and TiO_2, respectively, as shown in Figs. 2(a) and 2(b). One main advantage of XANES spectra lies in its sensitivity to the local symmetry, electronic structure and oxidation state of the absorbing atoms, thus. XANES pattern can be used as a fingerprint of the local environment around the absorbing atoms. As shown in the data for Fe *K*-edge, the position of absorption edge of all samples resembles the pattern for the Fe_2O_3 standard at 7125 eV, this shows that the oxidation state of Fe in Ba-doped BFO-BKT is +3. The Ti *K*-edge XANES spectra of all samples and the TiO_2 standard have an identical position of the absorption edge at 4980 eV, indicating that Ti species is +4. In addition, the measured Ba L3-edge XANES spectra and their first derivative is analyzed and compared with $BaCO_3$ standard, the data is shown in Fig. 2(c). It is clearly shown that the absorption edge of the samples and $BaCO_3$ standard is located at 5250 eV, indicating that the oxidation state of Ba is +2.

In order to identify the Ba site distribution in the 0.6BFO-0.4BKT system, Ba L_3-edge XANES spectra were simulated from the four possible models: 1) Ba substituted on the Bi site (A-site) of rhombohedral (or BFO lattice, Ba_{Bi_rhom}), and 2) tetragonal (or BKT lattice, Ba_{Bi_tetra}), and then 3) Ba replace the Fe site (B-site) of rhombohedral (Ba_{Fe_rhom}), and 4) Ba occupy at the Ti site (B-site) of tetragonal (Ba_{Ti_tetra}) perovskite structures compared with the calculated Ba L_3-edge XANES spectra of the different crystal structures of $BaTiO_3$ (Tetragonal structure) and $Pb_{0.8}Ba_{0.2}Zr_{0.65}Ti_{0.35}O_3$ (Rhombohedral structure) as reference materials. The atomic parameters used in the XANES calculation here were obtained from a prior study (Yoneda et al., 2012; Wefring et al., 2014; Mahmood et al., 2011; Mir et al., 2007), in which the global structure obtained from the X-ray diffraction (XRD) measurement.

The theoretical Ba L_3-edge XANES spectra were calculated using the FEFF8.2 program, which employs a full multiple scattering approaches based on self-consistent overlapping muffin-tin

potentials. The exchange-correlation function used in FEFF codes was Hedin-Lundqvist potential (Hedin and Lundqvist, 1969; Rher and Albers, 2000). The spherical cluster size of the electron wave function was increased until the spectra converged. The self-consistent calculations were performed in a cluster radius of 5.0 Å (about 50 atoms) around the absorbing Ba atom. The full multiple scattering calculations included all possible paths with a larger cluster radius of 7.5 Å (about 140 atoms) around the absorbing Ba atom.

The measured and calculated Ba *L*3-edge XANES spectra of Ba_{Bi_rhom}, Ba_{Bi_tetra}, Ba_{Fe_rhom}, Ba_{Ti_tetra} and reference materials are presented in Fig. 2(d). The main features of the measured XANES spectrum are composed of four peaks labeled as *P*1, *P*2, *P*3, and *P*4. These are consistent with the main peaks of the calculated Ba L_3-edge XANES spectra of Ba_{Bi_rhom} and Ba_{Bi_tetra}, while an improbable for Ba_{Fe_rhom} and Ba_{Ti_tetra}. Moreover, the features of the calculated XANES spectra of Ba_{Bi_rhom} and Ba_{Bi_tetra} seem to those of reference spectra, indicating that the local structure surrounding Ba atoms in BFO and BKT lattices is similar to that of Ba atoms in $BaTiO_3$ and $Pb_{0.8}Ba_{0.2}Zr_{0.65}Ti_{0.35}O_3$, respectively. This result confirm that Ba atoms can replace both A-sites of rhombohedral and tetragonal perovskite structures.

To determine the distribution of Ba substituting on both A-sites, the ratio of the main peaks of calculated XANES spectra of Ba_{Bi_rhom} and Ba_{Bi_tetra} was investigated, which using the linear combination analysis (LCA) method. Figure 2(e) and 2(f) show a comparison between the measured spectra and that of calculated for a linear combination with various proportions of Ba_{Bi_rhom} and Ba_{Bi_tetra} sites. One can easily see that the calculated XANES spectra are in very good agreement with the corresponding features in the measured spectra of ceramic samples in both energy positions and shapes, this implies that Ba atoms substitute in A-site of 0.6BFO-0.4BKT samples with the proportion of 70% on A-site of tetragonal (BKT lattice) and 30% on A-site of rhombohedral (BFO lattice) perovskite structures, not detectable by a conventional XRD measurement.

Temperature dependences on the dielectric constant (ε_r) of the Ba-doped 0.6BFO-0.4BKT ceramics with different Ba contents (0, 1, 3, 5, 7, and 10 mol%), are shown in Fig. 3. The maximum dielectric constant (ε_m) at 10 kHz tends to increase with increasing Ba contents. The data showed a board range at the maximum transition temperature, which belongs to a relaxor ferroelectric behavior similar to the finding in previous works (Yao et al., 2009). The Ba dopant has introduced charged defects which disturbs the long-range coupling between BO_6 octahedra in the perovskite structure (Yao et al., 2009; Levin et al., 2006). According to the Kröger–Vink notation, this can be responsible for the relaxation shown on the results (Yao et al., 2009).

In addition, a clear transition temperature when the dielectric constant is maximum (ε_r) at 10 kHz (defined as T_m) is identified. It is noticed that the T_m increase with increasing Ba contents up to

5 mol% and then decreases at 7 and 10 mol%, as shown in Fig. 3(b). This change of trend is most likely associated with the distortion in the crystal structure and switch between the order/disorder behavior of the materials (Kumar et al., 2008). This behavior could reveal the morphotropic phase boundary (MPB) between the tetragonal and rhombohedral phases for Ba-doped 0.6BFO-0.4BKT ceramics system, a similar behavior was reported in previous works (Matsuo et al., 2010; Wu et al., 2008). The result suggests that the transition temperature of Ba-doped 0.6BFO-0.4BKT ceramics system can be varied over a range from 380 to 500 °C by controlling the Ba content in the system, this agrees with other works. (Prasatkhetragarn and Yimnirun, 2013).

Room temperature (RT) magnetization of the samples with different Ba contents (0, 1, 3, 5, 7, and 10 mol%) as a function of the applied magnetic field (ranged between ± 10 kOe) are shown in Fig. 4. The data shows that the magnetization of undoped 0.6BFO-0.4BKT varied linearly with the applied magnetic field reflecting its antiferromagnetic characteristics (Matsuo et al., 2010; Kim et al., 2010; Prasatkhetragarn and Yimnirun, 2013). These antiferromagnetic natures are also displayed in samples with 1 to 3 mol% Ba contents. However, the remnant magnetization (M_r) and the coercive field (H_c) are also seen to increase with increasing Ba content, it reached the maximum values at 5 mol% ($M_r \approx 0.2$ emu/g, $H_c \approx 3$ kOe), then decreased till 10 mol%. The slim *M-H* hysteresis loops observed on the data with samples of 5 to 10 mol% of Ba dopant resemble the soft ferromagnetic behavior. In fact, $BiFeO_3$ is known to be antiferromagnetic with a G-type magnetic structure, it has a residual magnetic moment due to a cant spin structure (weak ferromagnetic) (Prasatkhetragarn and Yimnirun, 2013). This behavior was detected in the undoped BFO-BKT ceramics. The Ba-doped specimen reported here exhibits a clear magnetic hysteresis loop, indicating a soft ferromagnetic behavior. The appearance of ferromagnetism in solid solution systems could be attributed to the canting of the antiferromagnetically ordered spins by a structural distortion or the breakdown of the balance between the antiparallel sublattice magnetization of Fe^{3+} due to metal ion substitution with a different valence (Kumar et al., 2008; Prasatkhetragarn and Yimnirun, 2013).

4. Conclusions

Polycrystalline ceramics $0.6BiFeO_3–0.4Bi_{0.5}K_{0.5}TiO_3$, with different Ba-doping contents (1, 3, 5, 7 and 10 mol%) have been fabricated through a solid-state reaction technique. The local structure, dielectric and magnetic properties of the specimens are investigated by XRD and X-ray Absorption Near Edge Spectroscopy (XANES). XRD results show that the single-phase perovskite for all the ceramics, the coexistence of tetragonal and rhombohedral phase for undoped 0.6BFO–0.4BKT and the rhombohedral phase in the ceramics with increasing Ba content. The XANES results identified that the oxidation state of Fe, Ti, and Ba ions in 0.6BFO–0.4BKT system was +3, +4 and

+2, respectively. The results comparing the measured and calculated linear combination of Ba L3-edge XANES spectra indicate that the majority of Ba atoms occupy A-site in BKT lattice (tetragonal phase). Based on the dielectric measurement, the morphotropic phase boundary (MPB) between the tetragonal and rhombohedral phases is observed at 5 mol% content of Ba. The work also shows that the soft ferromagnetic properties are at an optimized level with 5 mol% Ba dopants.

Acknowledgement

This work was financially supported by the Thailand Research Fund (TRF) under the TRF Research Career Grant No. RSA5880056. This research was also supported by Unit of Excellence on Sensors Technology Grant No. UoE62006, School of Science, University of Phayao and Siam Photon Laboratory, Synchrotron Light Research Institute (SLRI), Thailand. This joint work has also received support from the European Union's Horizon 2020 research and innovation program under the Marie Skłodowska-Curie grant agreement "PRIGeoC" (No 689857).

References

[1] Yoneda, Y., Kitanaka, Y., Noguchi, Y., Miyayama M., 2012. Electronic and local structures of Mn-doped $BiFeO_3$ crystals, Phys. Rev. B. 86, 184112.

[2] Lee, S., Ratcliff, W., Cheong, S.-W., Kiryukhin, V., 2008. Electric field control of the magnetic state in $BiFeO_3$ single crystals, Appl. Phys. Lett. 92, 192906.

[3] Lebeugle, D., Colson, D., Forget, A., Viret, M., Bonville, P., Marucco, J.F., Fusil, S., 2007. Room-temperature coexistence of large electric polarization and magnetic order in $BiFeO_3$ single crystals, Phys. Rev. B. 76, 024116.

[4] Zhao, T., Scholl, A., Zavaliche, F., Lee, K., Barry, M., Doran, A., Cruz, M.P., Chu, Y.H., Ederer, C., Spaldin, N.A., Das, R.R., Kim, D.M., Baek, S.H., Eom, C.B., Ramesh, R., 2006. Electrical control of antiferromagnetic domains in multiferroic $BiFeO_3$ films at room temperature, Nat. Mater. 5, 823-829.

[5] Matsuo, H., Noguchi, Y., Miyayama, M., Suzuki, M., Watanabe, A., Sasabe, S., Ozaki, T., Mori, S., Torii, S., Kamiyama, T., 2010. Structural and piezoelectric properties of high-density $(Bi_{0.5}K_{0.5})TiO_3$–$BiFeO_3$ ceramics, J. Appl. Phys. 108, 104103.

[6] Kim, J.M., Sung, Y.S., Cho, J.H., Song, T.K., Kim, M.H., Chong, H.H., Park, T.G., Do, D., Kim, S.S., 2010. Piezoelectric and dielectric properties of lead-free $(1-x)(Bi_{0.5}K_{0.5})TiO_3$-$x BiFeO_3$ Ceramics, Ferroelectric. 404, 88-92.

[7] Wu, W., He, Q., Jiang, C., 2008. Magnetic iron oxide nanoparticles: synthesis and surface functionalization strategies, Nano. Res. Lett. 3, 397-415.

[8] Prasatkhetragarn, A., Arthan, A., Jantaratana, P., Vittayakorn, N., Yotburut, B., Yimnirun, R., 2013. Ferroelectromagnetic characteristic of Na-doped $0.75BiFeO_3$–$0.25BaTiO_3$ multiferroic ceramics, Ceram. Int. 39, 245-248.

[9] Dehkordi, A.M., Bhattacharya, S., Darroudi, T., Graff, J.W., Schwingenschlög, U., Alshareef, H.N., Tritt T.M., 2014. Large thermoelectric power factor in Pr-doped $SrTiO_{3-\delta}$ ceramics via grain-boundary-induced mobility enhancement, Chem. Mater. 26, 2478-2485.

[10] Yang, C., Tse, M.-Y, Wei, X., Hao, J., 2017. Colossal permittivity of (Mg + Nb) co-doped TiO_2 ceramics with low dielectric loss, J. Mater. Chem. C. 5, 5170-5175.

[11] Han, H.-S., Jo, W., Kang, J.-K., Ahn, C.-W., Kim, I.W., Ahn, K.-K., Lee, J.-S., 2013. Incipient piezoelectrics and electrostriction behavior in Sn-doped $Bi_{1/2}(Na_{0.82}K_{0.18})_{1/2}TiO_3$ lead-free ceramics, J. Appl. Phys. 113, 154102.

[12] Qin, Y.F., Yang, J., Huang, W.J., Xiong, P., Song, J.Y., Wang, D., Yin, L.H., Song, W.H., Tong, P., Zhu, X.B., Sun, Y.P., 2018. Effects of Co doping on structural, magnetic, and electrical properties of $0.6BiFeO_3$-$0.4(Bi_{0.5}K_{0.5})TiO_3$ solid solution, J. Alloy. Comp. 730, 119-126.

[13] Pan, D.-F., Zhou, M.-X., Lu, Z.-X., Zhang, H., Liu, J.-M., Wang, G.-H., Wan, J.-G., 2016. Local magnetoelectric effect in La-doped $BiFeO_3$ multiferroic thin films revealed by magnetic-field-assisted scanning probe microscopy, Nano. Res. Lett. 11, 318.

[14] Srinivas, V., Raghavender, A.T., Kumar, K.V., 2016. Structural and magnetic properties of Mn doped $BiFeO_3$ nanomaterials, Phys. Res. Int. 4835328.

[15] Wang, D., Khesro, A., Murakami, S., Feteira, A., Zhao, Q., Reaney, I.M., 2017. Temperature dependent, large electromechanical strain in Nd-doped $BiFeO_3$-$BaTiO_3$ lead-free ceramics, J. Eur. Ceram. Soc. 37, 1857-1860.

[16] Tuan, N.H., Bac, L.H., Cuong, L.V., Thiet, D.V., Tam. T.V., Dung, D.D., 2017. Structural, optical and magnetic properties of lead-free ferroelectric $Bi_{0.5}K_{0.5}TiO_3$ solid solution with $BiFeO_3$ materials, J. Electron. Mater. 46, 3472-3478.

[17] Yoon, M.-Y., Hwang, K.-J., Byeon, D.-S., Hwang, H.-J., Jeong, S.-M., 2014. Molecular dynamics simulation of the effect of dopant distribution homogeneity on the oxide ion conductivity of Ba-doped $LaInO_3$, J. Power. Source. 248, 1085-1089.

[18] Vagadia, M., Ravalia, A., Solanki, P.S., Choudhary, R.J., Phase, D.M., Kuberkar, D.G., 2013. Improvement in resistive switching of Ba-doped $BiFeO_3$ films, Appl. Phys. Lett. 103, 033504.

[19] Xie, Q.Y., Xie, W.M., Wang, J.L., Zhu, H.P., Yang, J.H., Sun, L., Wu, X.S., 2013. Detecting p-type conduction in Ba-doped InN, Appl. Phys. Lett. 102, 042109.

[20] Ravel, B., Newville, M., Data analysis for x-ray absorption spectroscopy using IFEFFIT, J. Synchro. Radiation. 12, 537-541.

[21] Wefring, E.T., Morozov, M.I., Einarsrud, M.-A., Grande, T., 2014. Dielectric and piezoelectric properties of solid solutions in the system (1-x)$Bi_{0.5}K_{0.5}TiO3$ – x$Bi_{0.5}Na_{0.5}ZrO_3$, J. Am. Ceram. Soc. 97, 2928-2935.

[22] Mahmood, N. B., Al- Shakarchi, E. K., 2011. Three techniques used to produce $BaTiO_3$ Fine powder, J. Mod. Phys. 2, 1420-1428.

[23] Mir, M., Mastelaro, V. R., Neves, P. P., Doriguetto, A. C., Garcia, D., Lente, M. H., Eiras, J. A., Mascarenhas, Y. P., 2007. X-ray powder diffraction structural characterization of $Pb_{1-x}Ba_xZr_{0.65}Ti_{0.35}O_3$ ceramic, Acta Cryst. B63, 713-718.

[24] Hedin, L., Lundqvist, S., 1969. Effects of electron-electron and electron-phonon interactions on the one-electron states of solids, Solid State Phys. 23, 1-181.

[25] Rher, J.J., Albers, R.C., 2000. Theoretical approaches to x-ray absorption fine structure, Rev. Mod. Phys. 72, 621-654.

[26] Yao, Z., Liu, H., Liu, Y., Chen, L., Hao, H., 2009. Structure and ferroelectric properties in $(K_{0.5}Bi_{0.5})TiO_3$–$BiScO_3$–$PbTiO_3$ piezoelectric ceramic system, Mater. Res. Bull. 44, 1511-1514.

[27] Levin, I., Cockayne, E., Lufaso, M.W., Woicik, J.C., Maslar, J.E., 2006. Local structures and raman spectra in the $Ca(Zr,Ti)O_3$ perovskite solid solutions, Chem. Mater. 18, 854-860.

[28] Kumar, A., Rivera, I., Katiyar, R.S., Scott, J.F., 2008, Multiferroic $Pb(Fe_{0.66}W_{0.33})_{0.80}Ti_{0.20}O_3$ thin films: A room-temperature relaxor ferroelectric and weak ferromagnetic, Appl. Phys. Lett. 92, 132913.

[29] Prasatkhetragarn, A., Yimnirun, R., 2013. Phase formation, electrical properties and morphotropic phase boundary of 0.95$Pb(Zr_xTi_{1-x})O_3$–0.05$Pb(Mn_{1/3}Nb_{2/3})O_3$ ceramics, Ceram. Int. 39, 91-95.

List of Figures

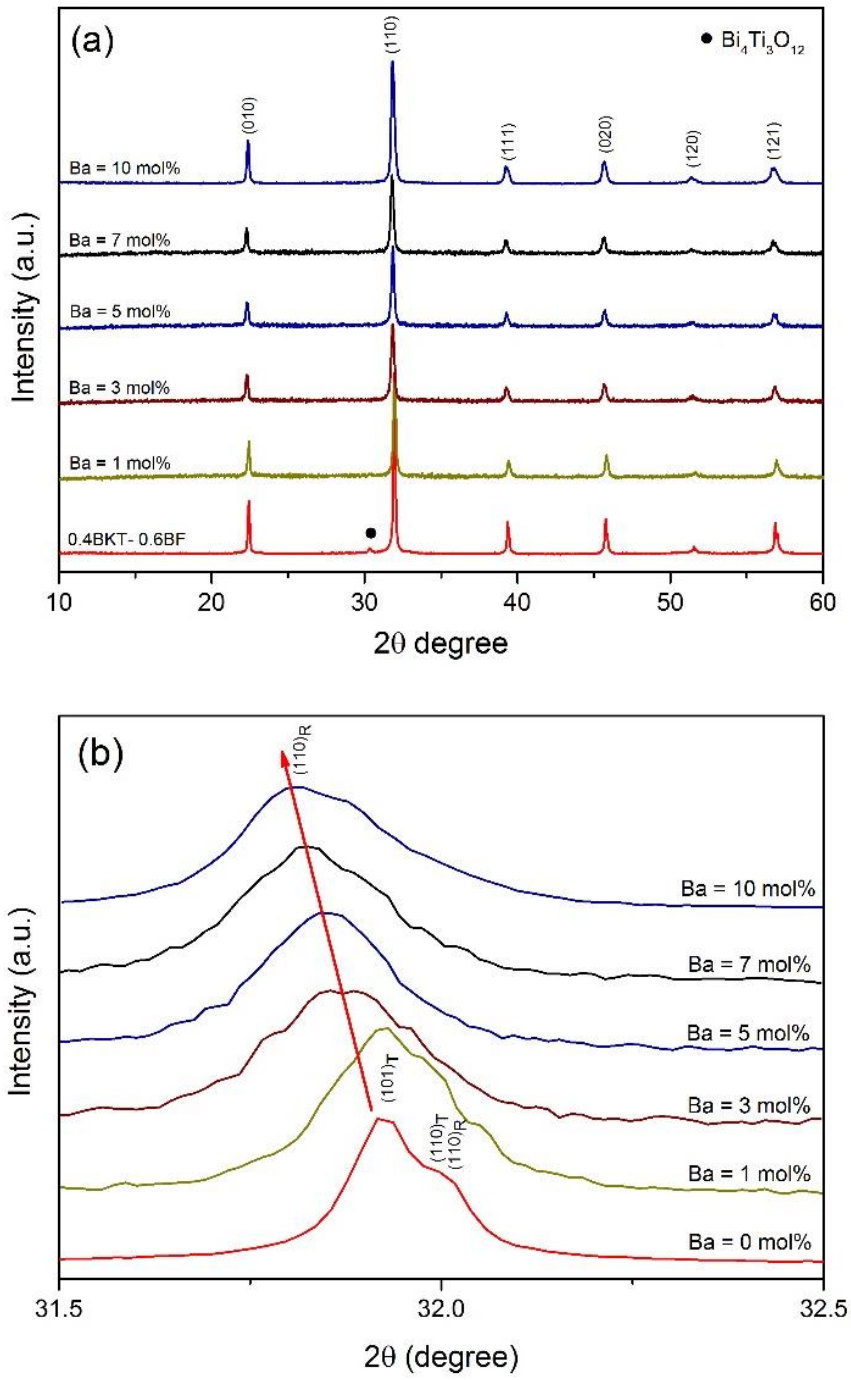
(a)
● $Bi_4Ti_3O_{12}$
(010)
(110)
(111)
(020)
(120)
(121)
Ba = 10 mol%
Ba = 7 mol%
Ba = 5 mol%
Ba = 3 mol%
Ba = 1 mol%
0.4BKT- 0.6BF
Intensity (a.u.)
10
20
30
40
50
60
2θ degree
(b)
$(110)_R$
$(101)_T$
$(110)_T$
$(110)_R$
Ba = 10 mol%
Ba = 7 mol%
Ba = 5 mol%
Ba = 3 mol%
Ba = 1 mol%
Ba = 0 mol%
Intensity (a.u.)
31.5
32.0
32.5
2θ (degree)

Fig. 1

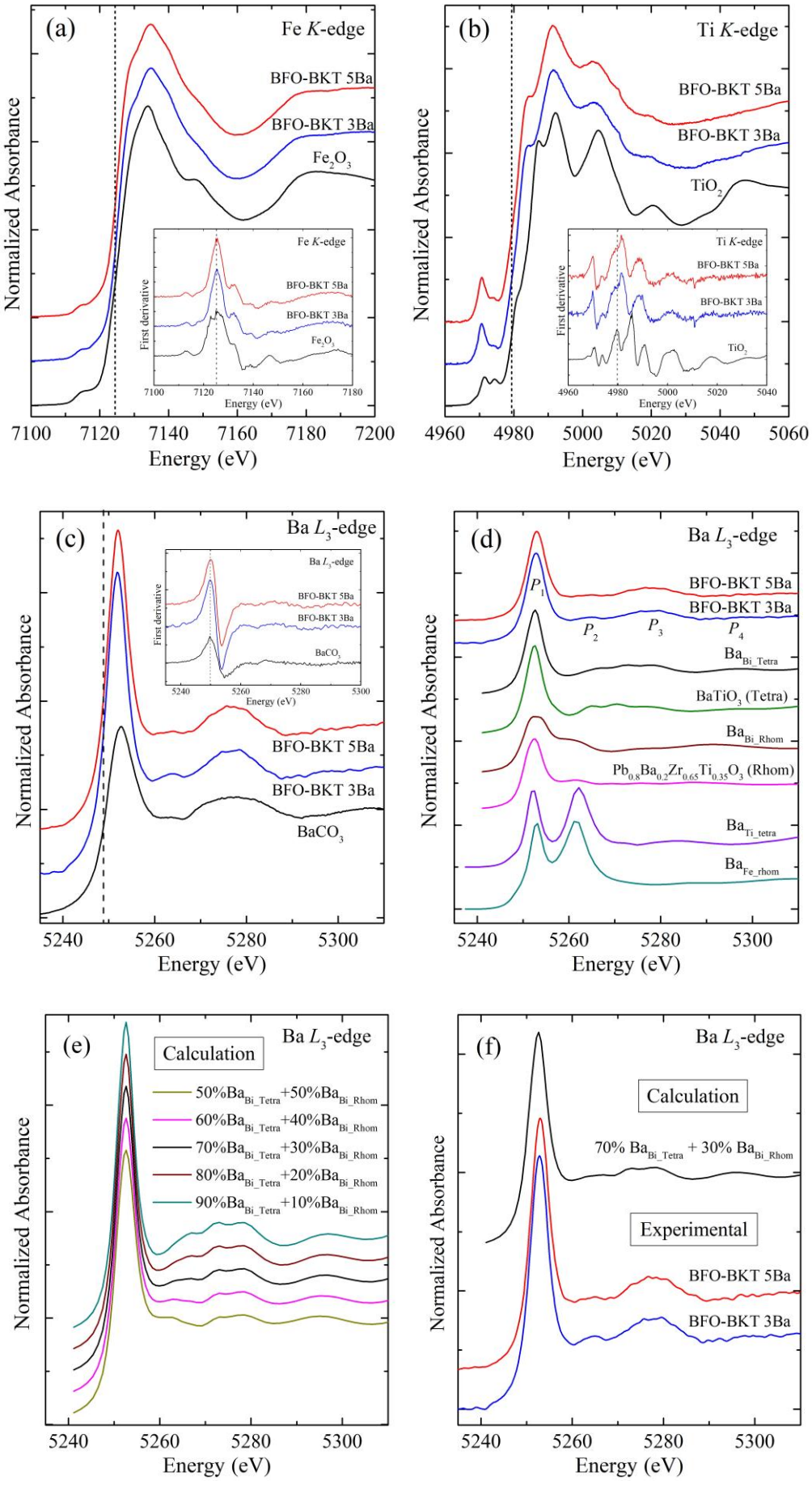
(a)
Fe K-edge
BFO-BKT 5Ba
BFO-BKT 3Ba
Fe2O3
Normalized Absorbance
Energy (eV)
First derivative
(b)
Ti K-edge
BFO-BKT 5Ba
BFO-BKT 3Ba
TiO2
Normalized Absorbance
Energy (eV)
First derivative
(c)
Ba L3-edge
BFO-BKT 5Ba
BFO-BKT 3Ba
BaCO3
Normalized Absorbance
Energy (eV)
First derivative
(d)
Ba L3-edge
P1
P2
P3
P4
BFO-BKT 5Ba
BFO-BKT 3Ba
BaBi_Tetra
BaTiO3 (Tetra)
BaBi_Rhom
Pb0.8Ba0.2Zr0.65Ti0.35O3 (Rhom)
BaTi_tetra
BaFe_rhom
Normalized Absorbance
Energy (eV)
(e)
Ba L3-edge
Calculation
50%BaBi_Tetra+50%BaBi_Rhom
60%BaBi_Tetra+40%BaBi_Rhom
70%BaBi_Tetra+30%BaBi_Rhom
80%BaBi_Tetra+20%BaBi_Rhom
90%BaBi_Tetra+10%BaBi_Rhom
Normalized Absorbance
Energy (eV)
(f)
Ba L3-edge
Calculation
70% BaBi_Tetra + 30% BaBi_Rhom
Experimental
BFO-BKT 5Ba
BFO-BKT 3Ba
Normalized Absorbance
Energy (eV)

Fig. 2

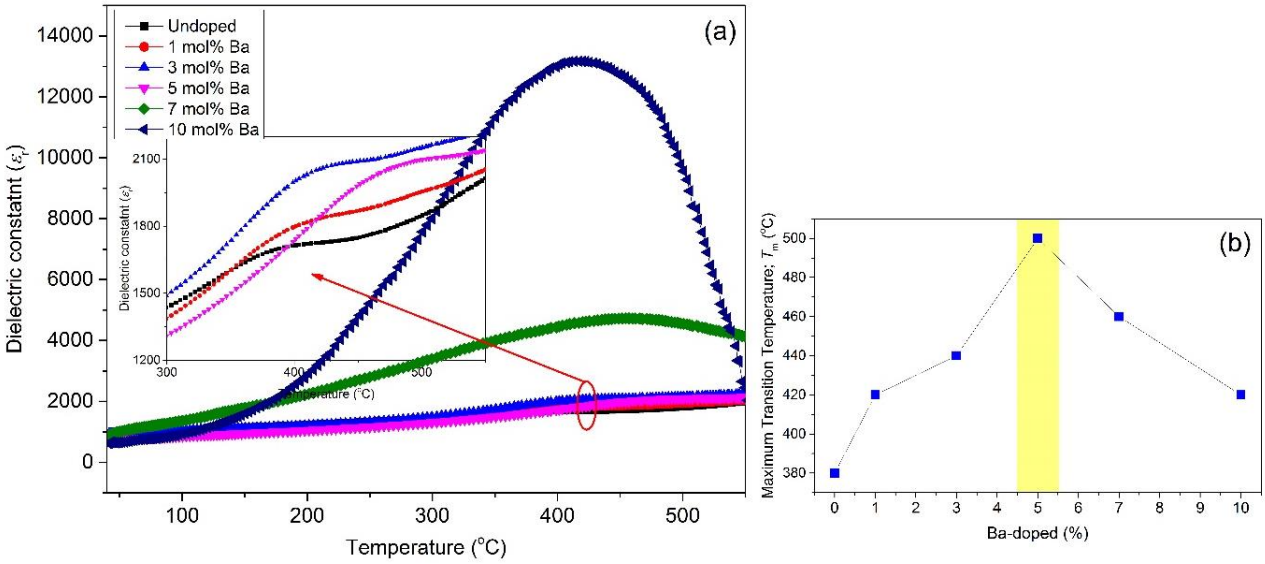
Undoped
1 mol% Ba
3 mol% Ba
5 mol% Ba
7 mol% Ba
10 mol% Ba
(a)
Dielectric constatnt (ε_r)
Temperature (°C)
(b)
Maximum Transition Temperature; T_m (°C)
Ba-doped (%)

Fig. 3

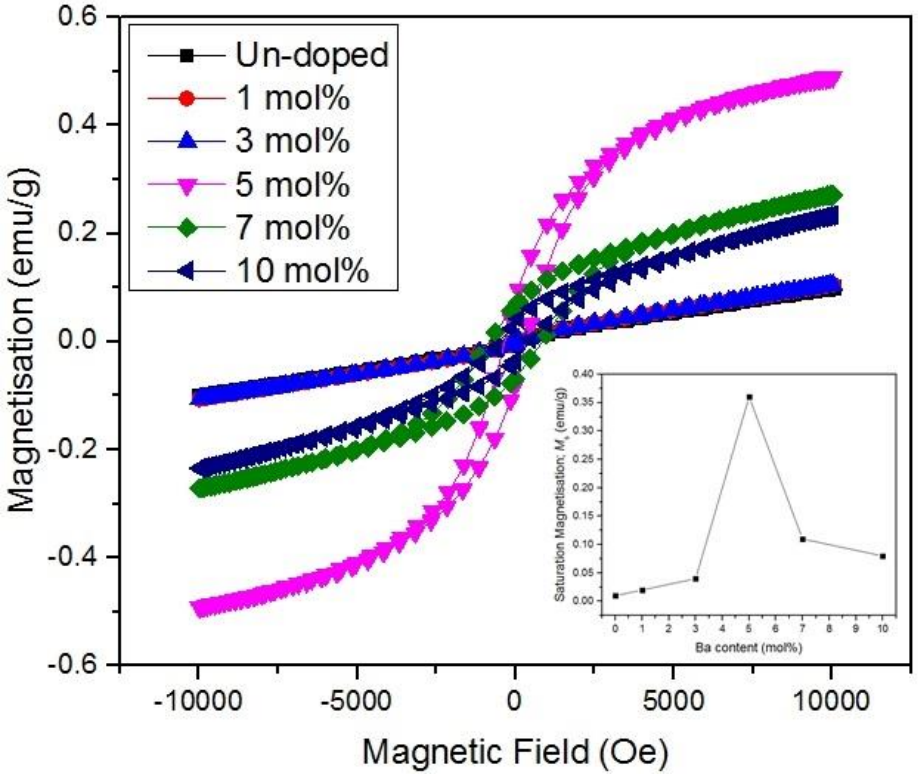
Un-doped
1 mol%
3 mol%
5 mol%
7 mol%
10 mol%
Magnetisation (emu/g)
Magnetic Field (Oe)
Saturation Magnetisation; M_s (emu/g)
Ba content (mol%)

Fig. 4